Green's function relativistic mean field theory for Λ hypernuclei

S.-H. Ren (任素红), T.-T. Sun (孙亭亭),* and W. Zhang (张炜)
School of Physics and Engineering, Zhengzhou University, Zhengzhou 450001, China
(Received 16 March 2017; published 22 May 2017)

The relativistic mean field theory with the Green's function method is extended to study Λ hypernuclei. Taking the hypernucleus ${}^{61}_{\Lambda}$Ca as an example, the single-particle resonant states for Λ hyperons are investigated by analyzing the density of states, and the corresponding energies and widths are given. Different behaviors are observed for the resonant states, i.e., the distributions of the very narrow $1f_{5/2}$ and $1f_{7/2}$ states are very similar to bound states while those of the wide $1g_{7/2}$ and $1g_{9/2}$ states are like scattering states. Besides, the impurity effect of Λ hyperons on the single-neutron resonant states is investigated. For most of the resonant states, both the energies and widths decrease with adding more Λ hyperons due to the attractive ΛN interaction. Finally, the energy level structure of Λ hyperons in the Ca hypernucleus isotopes with mass number $A = 53-73$ are studied; obvious shell structure and small spin-orbit splitting are found for the single-Λ spectrum.

DOI: 10.1103/PhysRevC.95.054318

I. INTRODUCTION

Since the first discovery of a Λ hypernucleus by Danysz and Pniewski in 1953 [1], the study of hypernuclei has been attracting great interest from nuclear physicists [2–5]. An important goal of hypernuclear physics is to extract information on the baryon-baryon interactions including the strangeness of freedom, which are crucial not only for the understanding of hypernuclear structure [6–9] but also for the study of neutron stars [10–13]. However, due to the difficulty of the hyperon-nucleon (YN) and hyperon-hyperon (YY) scattering experiments, there are very limited YN scattering data and no YY scattering data at all. Thus, in order to shed light on baryon-baryon interactions, the study of the hypernuclei structure is very important.

The most extensively studied hypernuclear system is the single-Λ hypernucleus which consists of one Λ hyperon coupled to a nuclear core. Until now, more than 30 Λ hypernuclei ranging from ${}^{3}_{\Lambda}$H up to ${}^{208}_{\Lambda}$Pb have been produced experimentally [2,3]. Several properties of hypernuclei such as the mass number dependence of single-Λ binding energy and spin-orbit splitting have been revealed. Double-Λ hypernuclei such as ${}^{6}_{\Lambda\Lambda}$He [14] have been observed experimentally and demonstrated the weakly attractive ΛΛ interaction by the small positive ΛΛ bond energy.

Being an additional strangeness degree of freedom, a hyperon is free from nucleon's Pauli exclusion principle, and it may induce many effects on the nuclear core as an impurity, such as the shrinkage of the size [15–17], the change of the shape [18,19], the modification of its cluster structure [20], the shift of neutron drip line to a neutron-rich side [21–23], and the occurrence of nucleon and hyperon skin or halo [20,22,24].

Theoretically, many different models have been contributed to study the structure of Λ hypernuclei, such as the cluster model [15,16,25,26], antisymmetrized molecular dynamics [27–30], shell model [31–34], mean field approaches [18,21,35–44], and *ab initio* method [45]. Among these methods, the mean field approach has an advantage in that it can be globally applied from light to heavy hypernuclei. Recently, both the Skyrme-Hartree-Fock (SHF) [35–39] and the relativistic mean field (RMF) models [18,21,40–44] have been applied to hypernuclear physics.

During the last few decades, the RMF model has achieved great success in ordinary nuclei [46–51]. In 1977, Brockmann and Weise applied this approach to hypernuclei [40]. At that time, it had been already observed experimentally that the spin-orbit splittings in hypernuclei are significantly smaller than those in ordinary nuclei [52]. The relativistic approach is suitable for a discussion of spin-orbit splittings in hypernuclei, because the spin-orbit interaction is naturally emerged with the relativistic framework. It has been applied to describe single- and multi-Λ systems, including the single-particle (s.p.) spectra of Λ hypernuclei and the spin-orbit interaction, and extended beyond the Λ to other strange baryons using SU(3) [7,21,42,53–62].

Hyperon halos may occur with the rapid development of radioactive ion beam facilities. For the halo structure, continuum and resonant states play crucial roles, especially those with low orbital angular momenta l [50,63–65]. For example, in ordinary nuclei, further studies have shown that the s.p. resonant states are key factors to many exotic nuclear phenomena, such as the halo [64,66], giant halo [65,67–71], and deformed halo [72,73]. To study the s.p. resonant states, many techniques have been developed based on conventional scattering theory [74–81] or the bound-state-like methods [82–84]. Meanwhile, combinations of a number of techniques for the s.p. resonant states with the RMF theory have been developed. For example, the RMF theory with the S-matrix (RMF-S) [78], the RMF theory with the analytic continuation in the coupling constant approach (RMF-ACCC) [85–88], the RMF theory with the real stabilization method (RMF-RSM) [89], the RMF theory with complex scaling method (RMF-CSM) [90], and the RMF theory with Green's function method (RMF-GF) [91,92].

Green's function method [93,94] has been demonstrated to be an efficient tool for describing the s.p. resonant states [91,92]. It has been widely applied in nuclear physics to

*ttsunphy@zzu.edu.cn

properly take into account the continuum, e.g., the ground state studies based on (nonrelativistic) Hartree-Fock-Bogoliubov (HFB) theory [95–98], and the excited state studies based on the quasiparticle random-phase-approximation (QRPA) theory [99,100] and the relativistic continuum random-phase-approximation (RCRPA) theory [101,102]. It is found that the Green's function method has the following advantages: (a) treating the discrete bound states and the continuum on the same footing, (b) giving both the energies and widths of the resonant states directly, and (c) taking into account the correct asymptotic behaviors for the wave functions.

In this paper, we extend the RMF-GF model to include the Λ hyperon in coordinate space and present detailed formulas of ΛN interaction and construction of Green's function for Λ hyperons. We apply this newly developed theory to three cases. First, taking ${}^{61}_{\Lambda}$Ca as an example, we apply the RMF-GF model to study the single-Λ resonant states. By analyzing the density of states, the s.p. energies for bound states and energies and widths for the resonant states are given. Second, taking ^{60}Ca, ${}^{61}_{\Lambda}$Ca, and ${}^{62}_{2\Lambda}$Ca as examples, we investigate the impurity effect of the Λ particle and focus on the influences of Λ hyperons on the single-neutron resonant states. Third, the s.p. level for Λ hyperon in the Ca hypernucleus isotopes are given and the shell structure and spin-orbit splitting are discussed.

The paper is organized as follows. In Sec. II, we present the formalism of the RMF-GF model for Λ hypernuclei. After the numerical details in Sec. III, we present the results and discussions in Sec. IV. Finally a summary is drawn in Sec. V.

II. THEORETICAL FRAMEWORK

A. RMF model for Λ hypernuclei

The starting point of the meson-exchange RMF model for Λ hypernuclei is a covariant Lagrangian density

$$\mathcal{L} = \mathcal{L}_N + \mathcal{L}_\Lambda \,, \tag{1}$$

where $\mathcal{L}_N$ is the standard RMF Lagrangian density for nucleons [48,50,51,103], and $\mathcal{L}_\Lambda$ is the Lagrangian density for Λ hyperons [42]. Since the Λ hyperon is charge neutral with isospin 0, only the couplings with σ and ω mesons are included,

$$\mathcal{L}_\Lambda = \bar{\psi}_\Lambda \Big[i\gamma^\mu \partial_\mu - m_\Lambda - g_{\sigma\Lambda}\sigma - g_{\omega\Lambda}\gamma^\mu \omega_\mu - \frac{f_{\omega\Lambda}}{2m_\Lambda}\sigma^{\mu\nu}\partial_\nu \omega_\mu \Big] \psi_\Lambda , \tag{2}$$

where m_Λ is the mass of the Λ hyperon, and $g_{\sigma\Lambda}$ and $g_{\omega\Lambda}$ are the coupling constants with the σ and ω mesons, respectively. The last term in $\mathcal{L}_\Lambda$ is the tensor coupling with the ω field [104], which is related to the s.p. spin-orbit splitting of Λ hyperons.

For a system with time-reversal symmetry, the space-like components of the vector ω_μ field vanish, only leaving the time components ω_0. With the mean field and no-sea approximations, the s.p. Dirac equations for baryons and the Klein-Gordon equations for mesons and photons can be obtained by the variational procedure.

The Dirac equation for Λ hyperon is

$$[\boldsymbol{\alpha}\cdot\boldsymbol{p} + \beta(m_\Lambda + S(\boldsymbol{r})) + V(\boldsymbol{r}) + T(\boldsymbol{r})]\psi_{i,\Lambda}(\boldsymbol{r}) = \varepsilon_i \psi_{i,\Lambda}(\boldsymbol{r}), \tag{3}$$

where $\boldsymbol{\alpha}$ and β are the Dirac matrices, $S(\boldsymbol{r})$, $V(\boldsymbol{r})$, and $T(\boldsymbol{r})$ are the scalar, vector, and tensor potentials for Λ hyperons, respectively, and

$$S = g_{\sigma\Lambda}\sigma, \tag{4a}$$

$$V = g_{\omega\Lambda}\omega_0, \tag{4b}$$

$$T = -\frac{f_{\omega\Lambda}}{2m_\Lambda} i\boldsymbol{\gamma}\cdot\boldsymbol{\nabla}\omega_0, \tag{4c}$$

with the $\boldsymbol{\gamma}$ matrix, i.e., $\gamma^k = \begin{pmatrix} 0 & \sigma^k \\ -\sigma^k & 0 \end{pmatrix}$ where k runs from 1 to 3 and σ^k are Pauli matrices.

The Klein-Gordon equations for the σ and ω mesons are changed to

$$\left(-\Delta + m_\phi^2\right)\phi = S_\phi, \tag{5}$$

with the source terms

$$S_\phi = \begin{cases} -g_\sigma \rho_S - g_{\sigma\Lambda}\rho_{S\Lambda} - g_2\sigma^2 - g_3\sigma^3 & \text{for } \sigma, \\ g_\omega \rho_V + g_{\omega\Lambda}\rho_{V\Lambda} + \dfrac{f_{\omega\Lambda}}{2m_\Lambda}\partial_k \boldsymbol{j}^{0k}_{T\Lambda} - c_3\omega_0^3 & \text{for } \omega, \end{cases} \tag{6}$$

where $m_\phi(\phi = \sigma,\omega)$ are the corresponding meson masses, g_σ, g_ω, g_2, g_3, and c_3 are the parameters for the nucleon-nucleon (NN) interaction in the Lagrangian density $\mathcal{L}_N$, $\rho_S(\rho_{S\Lambda})$, $\rho_V(\rho_{V\Lambda})$ are the scalar and baryon densities for the nucleons(hyperons), respectively, and $\boldsymbol{j}^0_{T\Lambda}$ is the tensor density for Λ hyperons.

With the upper $G_{i,\Lambda}(\boldsymbol{r})$ and lower $F_{i,\Lambda}(\boldsymbol{r})$ components of the Dirac spinor $\psi_{i,\Lambda}(\boldsymbol{r})$, the densities for Λ hyperons can be expressed as

$$\rho_{S\Lambda}(\boldsymbol{r}) = \sum_{i=1}^{A_\Lambda}[G_{i,\Lambda}(\boldsymbol{r})G^*_{i,\Lambda}(\boldsymbol{r}) - F_{i,\Lambda}(\boldsymbol{r})F^*_{i,\Lambda}(\boldsymbol{r})], \tag{7a}$$

$$\rho_{V\Lambda}(\boldsymbol{r}) = \sum_{i=1}^{A_\Lambda}[G_{i,\Lambda}(\boldsymbol{r})G^*_{i,\Lambda}(\boldsymbol{r}) + F_{i,\Lambda}(\boldsymbol{r})F^*_{i,\Lambda}(\boldsymbol{r})], \tag{7b}$$

$$\boldsymbol{j}^0_{T\Lambda}(\boldsymbol{r}) = \sum_{i=1}^{A_\Lambda}[G_{i,\Lambda}(\boldsymbol{r})F^*_{i,\Lambda}(\boldsymbol{r}) + F_{i,\Lambda}(\boldsymbol{r})G^*_{i,\Lambda}(\boldsymbol{r})]\boldsymbol{n}, \tag{7c}$$

where $\boldsymbol{n}$ is the angular unit vector. The number of Λ hyperons A_Λ is calculated by the integral of the hyperon density $\rho_{V\Lambda}(\boldsymbol{r})$ in the coordinate space as

$$A_\Lambda = \int d^3r \rho_{V\Lambda}(\boldsymbol{r}). \tag{8}$$

And the total baryon (mass) number A in hypernuclei is the summation of the neutron, proton, and Λ hyperon particle numbers.

The Dirac equation for nucleons and Klein-Gordon equations for ρ mesons and photons are the same as those in the standard RMF model. All these coupled equations together

with Eqs. (3)–(8) are solved by iteration in the coordinate space.

B. Green's function method

Green's function $\mathcal{G}(\boldsymbol{r},\boldsymbol{r}';\varepsilon)$ describes the propagation of a particle with an energy ε from coordinate $\boldsymbol{r}$ to $\boldsymbol{r}'$. In the RMF-GF theory [91,92], the Green's function method is taken to solve the Dirac equation in coordinate space, and the relativistic s.p. Green's function obeys

$$[\varepsilon - \hat{h}(\boldsymbol{r})]\mathcal{G}(\boldsymbol{r},\boldsymbol{r}';\varepsilon) = \delta(\boldsymbol{r}-\boldsymbol{r}'), \tag{9}$$

where $\hat{h}(\boldsymbol{r})$ is the Dirac Hamiltonian, and energy ε can be any value on a energy complex plane. For Λ hyperons, $\hat{h}(\boldsymbol{r}) = \boldsymbol{\alpha}\cdot\boldsymbol{p} + \beta(m_\Lambda + S(\boldsymbol{r})) + V(\boldsymbol{r}) + T(\boldsymbol{r})$. With a complete set of eigenstates $\psi_{i,\Lambda}(\boldsymbol{r})$ and eigenvalues ε_i, Green's function for Λ hyperons can be represented as

$$\mathcal{G}(\boldsymbol{r},\boldsymbol{r}';\varepsilon) = \sum_i \frac{\psi_{i,\Lambda}(\boldsymbol{r})\psi^\dagger_{i,\Lambda}(\boldsymbol{r}')}{\varepsilon-\varepsilon_i}, \tag{10}$$

where Σ_i is summation for the discrete states and integral for the continuum explicitly. Green's function in Eq. (10) is analytic on the complex energy plane with the poles at eigenvalues ε_i. Corresponding to the upper $G_{i,\Lambda}(\boldsymbol{r})$ and lower $F_{i,\Lambda}(\boldsymbol{r})$ components of the Dirac spinor $\psi_{i,\Lambda}(\boldsymbol{r})$, Green's function for the Dirac equation is in a form of a 2×2 matrix,

$$\mathcal{G}(\boldsymbol{r},\boldsymbol{r}';\varepsilon) = \begin{pmatrix} \mathcal{G}^{(11)}(\boldsymbol{r},\boldsymbol{r}';\varepsilon) & \mathcal{G}^{(12)}(\boldsymbol{r},\boldsymbol{r}';\varepsilon) \\ \mathcal{G}^{(21)}(\boldsymbol{r},\boldsymbol{r}';\varepsilon) & \mathcal{G}^{(22)}(\boldsymbol{r},\boldsymbol{r}';\varepsilon) \end{pmatrix}. \tag{11}$$

According to Cauchy's theorem, the nonlocal scalar density $\rho_{S\Lambda}(\boldsymbol{r},\boldsymbol{r}')$, vector density $\rho_{V\Lambda}(\boldsymbol{r},\boldsymbol{r}')$, and tensor density $\boldsymbol{j}^0_{T\Lambda}(\boldsymbol{r},\boldsymbol{r}')$ for Λ hyperons can be calculated by the integrals of Green's function on the complex energy plane,

$$\begin{aligned}\rho_{S\Lambda}(\boldsymbol{r},\boldsymbol{r}') &= \sum_{i=1}^{A_\Lambda}[G_{i,\Lambda}(\boldsymbol{r})G^*_{i,\Lambda}(\boldsymbol{r}') - F_{i,\Lambda}(\boldsymbol{r})F^*_{i,\Lambda}(\boldsymbol{r}')] \\ &= \frac{1}{2\pi i}\oint_{C_\varepsilon} d\varepsilon[\mathcal{G}^{(11)}(\boldsymbol{r},\boldsymbol{r}';\varepsilon) - \mathcal{G}^{(22)}(\boldsymbol{r},\boldsymbol{r}';\varepsilon)],\end{aligned} \tag{12a}$$

$$\begin{aligned}\rho_{V\Lambda}(\boldsymbol{r},\boldsymbol{r}') &= \sum_{i=1}^{A_\Lambda}[G_{i,\Lambda}(\boldsymbol{r})G^*_{i,\Lambda}(\boldsymbol{r}') + F_{i,\Lambda}(\boldsymbol{r})F^*_{i,\Lambda}(\boldsymbol{r}')] \\ &= \frac{1}{2\pi i}\oint_{C_\varepsilon} d\varepsilon[\mathcal{G}^{(11)}(\boldsymbol{r},\boldsymbol{r}';\varepsilon) + \mathcal{G}^{(22)}(\boldsymbol{r},\boldsymbol{r}';\varepsilon)],\end{aligned} \tag{12b}$$

$$\begin{aligned}\boldsymbol{j}^0_{T\Lambda}(\boldsymbol{r},\boldsymbol{r}') &= \sum_{i=1}^{A_\Lambda}[G_{i,\Lambda}(\boldsymbol{r})F^*_{i,\Lambda}(\boldsymbol{r}') + F_{i,\Lambda}(\boldsymbol{r})G^*_{i,\Lambda}(\boldsymbol{r}')]\boldsymbol{n} \\ &= \frac{1}{2\pi i}\oint_{C_\varepsilon} d\varepsilon[\mathcal{G}^{(12)}(\boldsymbol{r},\boldsymbol{r}';\varepsilon) + \mathcal{G}^{(21)}(\boldsymbol{r},\boldsymbol{r}';\varepsilon)]\boldsymbol{n},\end{aligned} \tag{12c}$$

where C_ε is the contour path for the integral of Green's function on the complex energy plane shown in Fig. 1.

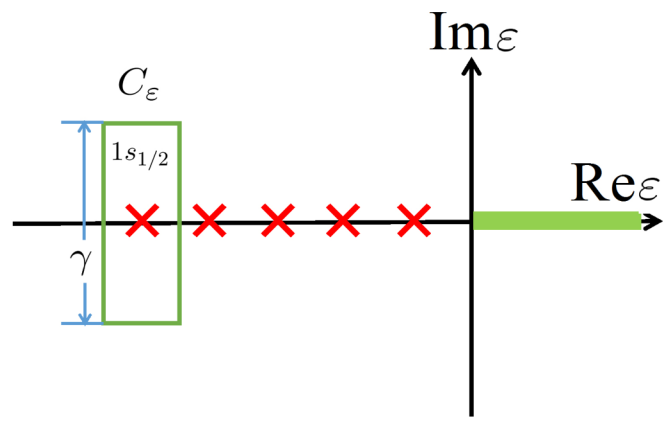

FIG. 1. Contour path C_ε to perform the integrals of Green's function on the complex energy plane. The path is chosen to be a rectangle with height γ and enclose only the $1s_{1/2}$ orbit. The red crosses denote the discrete single-Λ states and the green thick line denotes the continuum.

With the spherical symmetry, Green's function and densities can be expanded as radial and angular parts,

$$\mathcal{G}(\boldsymbol{r},\boldsymbol{r}';\varepsilon) = \sum_{\kappa m} Y^l_{jm}(\theta,\phi)\frac{\mathcal{G}_\kappa(r,r';\varepsilon)}{rr'}Y^{l*}_{jm}(\theta',\phi'), \tag{13a}$$

$$\rho_{S\Lambda}(\boldsymbol{r},\boldsymbol{r}') = \sum_{\kappa m} Y^l_{jm}(\theta,\phi)\rho_{S\Lambda,\kappa}(r,r')Y^{l*}_{jm}(\theta',\phi'), \tag{13b}$$

$$\rho_{V\Lambda}(\boldsymbol{r},\boldsymbol{r}') = \sum_{\kappa m} Y^l_{jm}(\theta,\phi)\rho_{V\Lambda,\kappa}(r,r')Y^{l*}_{jm}(\theta',\phi'), \tag{13c}$$

$$\boldsymbol{j}^0_{T\Lambda}(\boldsymbol{r},\boldsymbol{r}') = \sum_{\kappa m} Y^l_{jm}(\theta,\phi)\boldsymbol{j}^0_{T\Lambda,\kappa}(r,r')Y^{l*}_{jm}(\theta',\phi'). \tag{13d}$$

And they are only decided by the radial part, which is characterized by the quantum number $\kappa = (-1)^{j+l+1/2}(j+1/2)$ and orbits with the same κ is defined as a "block". The radial parts of the local scalar density $\rho_{S\Lambda}(\boldsymbol{r}) = \rho_{S\Lambda}(\boldsymbol{r},\boldsymbol{r})$, vector density $\rho_{V\Lambda}(\boldsymbol{r}) = \rho_{V\Lambda}(\boldsymbol{r},\boldsymbol{r})$, and tensor density $\boldsymbol{j}^0_{T\Lambda}(\boldsymbol{r}) = \boldsymbol{j}^0_{T\Lambda}(\boldsymbol{r},\boldsymbol{r})$ can be expressed by the radial part of Green's function as

$$\begin{aligned}\rho_{S\Lambda}(r) &= \frac{1}{4\pi r^2}\frac{1}{2\pi i}\sum_\kappa(2j+1) \\ &\quad\times\oint_{C_\varepsilon} d\varepsilon\big[\mathcal{G}^{(11)}_\kappa(r,r;\varepsilon) - \mathcal{G}^{(22)}_\kappa(r,r;\varepsilon)\big],\end{aligned} \tag{14a}$$

$$\begin{aligned}\rho_{V\Lambda}(r) &= \frac{1}{4\pi r^2}\frac{1}{2\pi i}\sum_\kappa(2j+1) \\ &\quad\times\oint_{C_\varepsilon} d\varepsilon\big[\mathcal{G}^{(11)}_\kappa(r,r;\varepsilon) + \mathcal{G}^{(22)}_\kappa(r,r;\varepsilon)\big],\end{aligned} \tag{14b}$$

$$\begin{aligned}\boldsymbol{j}^0_{T\Lambda}(r) &= \frac{1}{4\pi r^2}\frac{1}{2\pi i}\sum_\kappa(2j+1) \\ &\quad\times\oint_{C_\varepsilon} d\varepsilon\big[\mathcal{G}^{(12)}_\kappa(r,r;\varepsilon) + \mathcal{G}^{(21)}_\kappa(r,r;\varepsilon)\big]\boldsymbol{n},\end{aligned} \tag{14c}$$

Note that for the Λ hyperons occupying the $1s_{1/2}$ orbit, the degeneracy is $2j+1=2$. It is half occupied for single-Λ hypernuclei and fully occupied for double-Λ hypernuclei.

Different from the standard RMF model, in the RMF-GF model, from the densities given by Green's function (14), one can solve the Klein-Gordon equation (5) to obtain the σ and ω fields, and then calculate the single-Λ potentials $V(\boldsymbol{r})$, $S(\boldsymbol{r})$, and $T(\boldsymbol{r})$ in Eq. (4), and the Dirac equation is solved again to provide new Green's functions. In this way, the RMF coupled equations can be solved by iteration self-consistently.

In the RMF-GF theory, the energies of the s.p. bound states as well as the energies and widths of the s.p. resonant states can be extracted from the density of states $n(\varepsilon)$ [91,92],

$$n(\varepsilon)=\sum_i \delta(\varepsilon-\varepsilon_i), \tag{15}$$

where ε_i is the eigenvalue of the Dirac equation, ε is a real s.p. energy, $\sum_i$ includes the summation for the discrete states and the integral for the continuum, and $n(\varepsilon)d\varepsilon$ gives the number of states in the interval $[\varepsilon,\varepsilon+d\varepsilon]$. For the bound states, the density of states $n(\varepsilon)$ exhibits a discrete δ function at $\varepsilon=\varepsilon_i$, while in the continuum $n(\varepsilon)$ has a continuous distribution.

In the spherical case, Eq. (15) becomes

$$n(\varepsilon)=\sum_\kappa n_\kappa(\varepsilon), \tag{16}$$

where $n_\kappa(\varepsilon)$ is the density of states for a block characterized by the quantum number κ. By introducing an infinitesimal imaginary part $i\epsilon$ to energy ε, it can be proved that the density of states can be obtained by integrating the imaginary part of Green's function over the coordinate space, and in the spherical case, it is [91]

$$n_\kappa(\varepsilon)=-\frac{2j+1}{\pi}\int dr\,\mathrm{Im}\big[\mathcal{G}_\kappa^{(11)}(r,r;\varepsilon+i\epsilon) + \mathcal{G}_\kappa^{(22)}(r,r;\varepsilon+i\epsilon)\big]. \tag{17}$$

Moreover, with this infinitesimal imaginary part $i\epsilon$, the density of states for discrete s.p. states in shape of a δ function (no width) is simulated by a Lorentzian function with the FWHM of 2ϵ.

C. Construction of Green's function

In the spherical case, for a given single-Λ energy ε and quantum number κ, Green's function $\mathcal{G}_\kappa(r,r';\varepsilon)$ for the radial form of the Dirac equation (3) can be constructed as [91,92,94,101,102]

$$\mathcal{G}_\kappa(r,r';\varepsilon)=\frac{1}{W_\kappa(\varepsilon)}\big[\theta(r-r')\phi_\kappa^{(2)}(r,\varepsilon)\phi_\kappa^{(1)\dagger}(r',\varepsilon) + \theta(r'-r)\phi_\kappa^{(1)}(r,\varepsilon)\phi_\kappa^{(2)\dagger}(r';\varepsilon)\big], \tag{18}$$

where $\theta(r-r')$ is the radial step function, $\phi_\kappa^{(1)}(r,\varepsilon)$ and $\phi_\kappa^{(2)}(r,\varepsilon)$ are two linearly independent Dirac spinors for Λ hyperons,

$$\phi_\kappa^{(1)}(r,\varepsilon)=\begin{pmatrix}G_\kappa^{(1)}(r,\varepsilon)\\ F_\kappa^{(1)}(r,\varepsilon)\end{pmatrix},\quad \phi_\kappa^{(2)}(r,\varepsilon)=\begin{pmatrix}G_\kappa^{(2)}(r,\varepsilon)\\ F_\kappa^{(2)}(r,\varepsilon)\end{pmatrix}, \tag{19}$$

and $W_\kappa(\varepsilon)$ is the Wronskian function defined by

$$W_\kappa(\varepsilon)=G_\kappa^{(1)}(r,\varepsilon)F_\kappa^{(2)}(r,\varepsilon)-G_\kappa^{(2)}(r,\varepsilon)F_\kappa^{(1)}(r,\varepsilon), \tag{20}$$

and it is independent with coordinate r, i.e., $dW_\kappa(\varepsilon)/dr=0$.

The Dirac spinor $\phi_\kappa^{(1)}(r)$ is regular at the origin and $\phi_\kappa^{(2)}(r)$ at $r\to\infty$ is oscillating outgoing for $\varepsilon>0$ and exponentially decaying for $\varepsilon<0$. Explicitly, the Dirac spinor $\phi_\kappa^{(1)}(r,\varepsilon)$ at $r\to 0$ satisfies

$$\phi_\kappa^{(1)}(r,\varepsilon)\longrightarrow r\begin{pmatrix} j_l(kr)\\ \frac{\kappa}{|\kappa|}\frac{\varepsilon-V-S}{k}j_{\tilde{l}}(kr)\end{pmatrix}, \longrightarrow \begin{pmatrix}\frac{r}{(2l+1)!!}(kr)^l\\ \frac{\kappa}{|\kappa|}\frac{r(\varepsilon-V-S)}{k(2\tilde{l}+1)!!}(kr)^{\tilde{l}}\end{pmatrix}, \tag{21}$$

where $k^2=(\varepsilon-V-S)(\varepsilon-V-S+2m_\Lambda)>0$, quantum number $\tilde{l}$ is defined as $\tilde{l}=l+(-1)^{j+l+1/2}$, and $j_l(kr)$ is the spherical Bessel function of the first kind.

The Dirac spinor $\phi_\kappa^{(2)}(r,\varepsilon)$ at $r\to\infty$ satisfies

$$\phi_\kappa^{(2)}(r,\varepsilon)\longrightarrow \begin{pmatrix} rh_l^{(1)}(kr)\\ \frac{\kappa}{|\kappa|}\frac{ikr}{\varepsilon+2m_\Lambda}h_{\tilde{l}}^{(1)}(kr)\end{pmatrix}, \longrightarrow \begin{pmatrix}1\\ \frac{\kappa}{|\kappa|}\frac{ik}{\varepsilon+2m_\Lambda}\end{pmatrix}e^{ikr}, \tag{22}$$

for $\varepsilon>0$ and

$$\phi_\kappa^{(2)}(r,\varepsilon)\longrightarrow \begin{pmatrix} r\sqrt{\frac{2Kr}{\pi}}K_{l+\frac{1}{2}}(Kr)\\ \frac{-Kr}{\varepsilon+2m_\Lambda}\sqrt{\frac{2Kr}{\pi}}K_{\tilde{l}+\frac{1}{2}}(Kr)\end{pmatrix}, \longrightarrow \begin{pmatrix}1\\ -\frac{K}{\varepsilon+2m_\Lambda}\end{pmatrix}e^{-Kr}, \tag{23}$$

for $\varepsilon<0$. Here, $K^2=(V-S-\varepsilon)(\varepsilon-V+S+2m_\Lambda)>0$, $h_l^{(1)}(kr)$ is the spherical Hankel function of the first kind, and $K_{l+\frac{1}{2}}(Kr)$ is the modified spherical Bessel function.

III. NUMERICAL DETAILS

In the present RMF-GF calculations, for the NN interaction, the effective interaction PK1 [105] is taken. For the ΛN interaction, with Λ hyperon mass $m_\Lambda=1115.6$ MeV, the scalar coupling constant $g_{\sigma\Lambda}=0.618g_\sigma$ is fixed to reproduce the experimental binding energies of Λ in the $1s_{1/2}$ state of hypernucleus ${}^{40}_{\Lambda}$Ca ($B_{1s}^{\Lambda}=18.7$ MeV) [106] based on the NN interaction; the vector coupling constant $g_{\omega\Lambda}=0.666g_\omega$ is determined from the näive quark model [107]; and the tensor coupling constant $f_{\omega\Lambda}=-1.0g_{\omega\Lambda}$ is taken as in Ref. [42] which is related to the spin-orbit splitting of Λ hyperons. With those NN and ΛN interactions, the single-Λ binding energy B_Λ for hypernuclei from ${}^{12}_{\Lambda}$C to ${}^{208}_{\Lambda}$Pb are well described and consistent results with the experimental data [2,3] are obtained as shown in Fig. 2.

The RMF Dirac equation is solved in a box of size $R=20$ fm and a step size of 0.05 fm. In the present work, single- or double-Λ hypernuclei are studied, in which the Λ hyperons occupy the $1s_{1/2}$ orbit. To perform the integrals of Green's function in Eq. (14), the contour path C_ε is chosen to be a

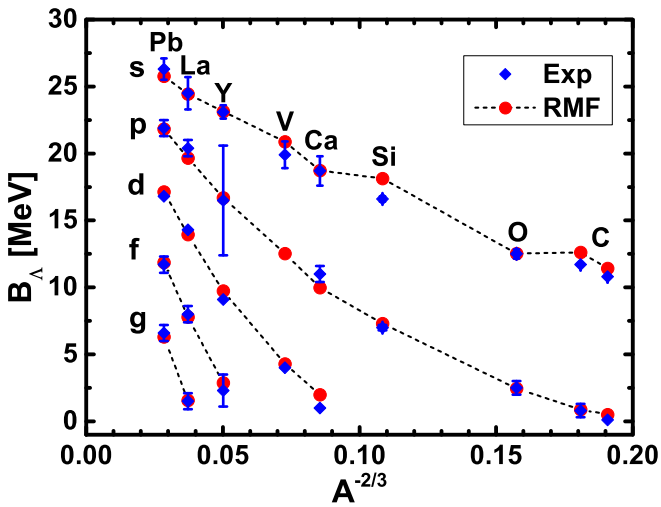

FIG. 2. Single-Λ binding energies B_Λ for the Λ hypernuclei from ${}^{12}_{\Lambda}$C to ${}^{208}_{\Lambda}$Pb calculated with the RMF-GF method and compared with the experimental data [2,3].

rectangle with height $\gamma = 0.1$ MeV and it encloses only the bound state $1s_{1/2}$ on the complex energy plane as shown in Fig. 1. The energy step is taken as $d\varepsilon = 0.005$ MeV on the contour path for the integral. With these parameters of the contour path C_ε, the convergence of the obtained densities for Λ hyperons in Eq. (14) is up to 10^{-14} fm^{-3}. To calculate the density of states $n_\kappa(\varepsilon)$ along the real-ε axis, the parameter ϵ in Eq. (17) is taken as 1×10^{-6} MeV and the energy step along the real-ε axis is 1×10^{-4} MeV. With this energy step, the accuracy for energies and widths of the s.p. resonant states can be up to 0.1 keV.

IV. RESULTS AND DISCUSSION

In this part, first we take ${}^{61}_{\Lambda}$Ca as an example and extend the RMF-GF model to investigate the s.p. spectrum of hypernuclei. In Fig. 3, the density of states $n_\kappa(\varepsilon)$ in different blocks κ for the Λ hyperon in hypernucleus ${}^{61}_{\Lambda}$Ca are plotted as a function of single-Λ energy ε. The dotted line in each panel indicates the continuum threshold. The peaks of the δ-functional shape below the continuum threshold correspond to bound states and spectra with $\varepsilon > 0$ are continuous. By comparing density of states for ${}^{61}_{\Lambda}$Ca (denoted by blue solid line) and those for free particles obtained with zero potential $V = S = 0$ (denoted by the red solid line), one can easily find the resonant states in the continuum. It is clear that the density of states $n_\kappa(\varepsilon)$ for the

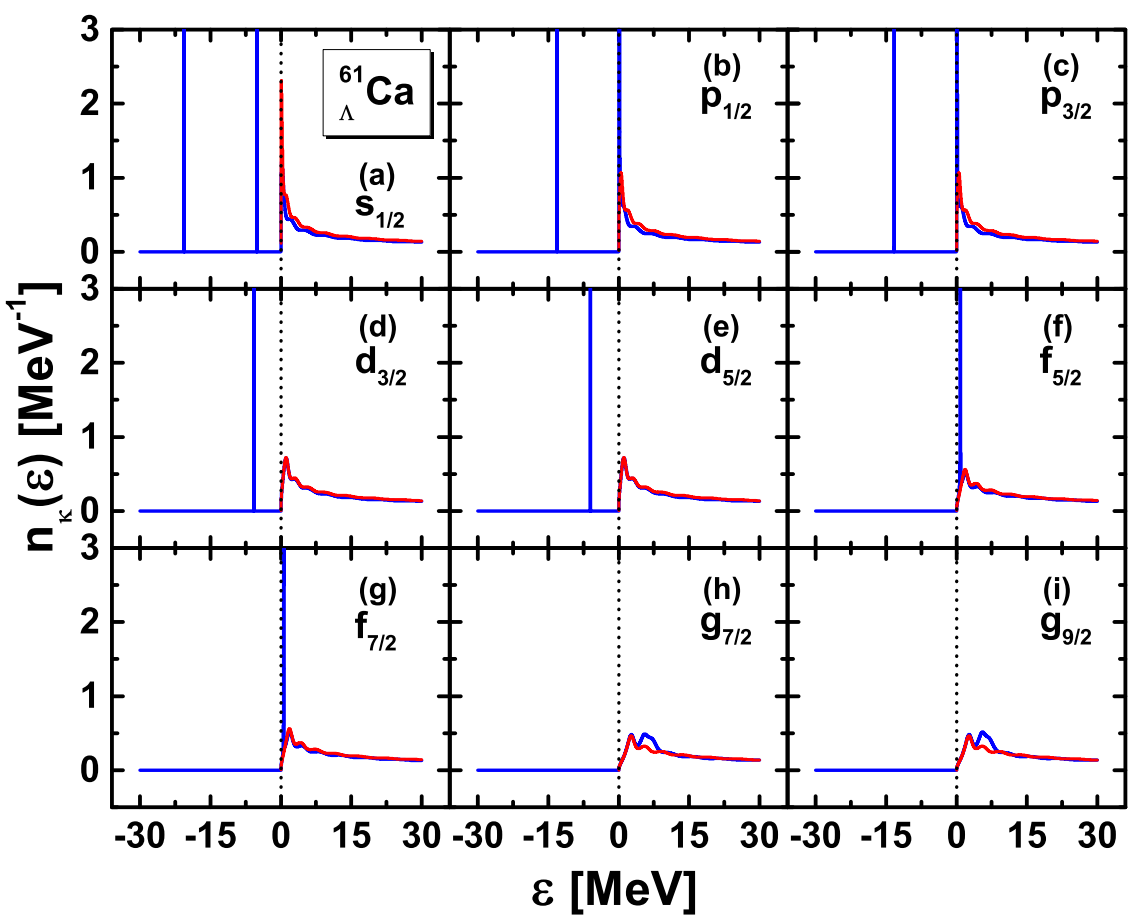

FIG. 3. Density of states $n_\kappa(\varepsilon)$ of Λ hyperon for different blocks κ in ${}^{61}_{\Lambda}$Ca calculated with RMF-GF method (blue solid line) and compared with $n_\kappa(\varepsilon)$ for free particles obtained with potentials $V = S = 0$ (red solid line). The dotted line in each panel indicates the position of the continuum threshold.

TABLE I. Single-Λ energies in ${}^{61}_{\Lambda}$Ca extracted from $n_\kappa(\varepsilon)$ in Fig. 3 by the RMF-GF method. Part (a) is for the bound states, in comparison with energies $\varepsilon_{\rm box}$ obtained by the shooting method with the box boundary condition. Part (b) is for the resonant states, where both the energies $\varepsilon_{\rm res.}$ and widths Γ are listed. All quantities are in MeV.

(a)	$1s_{1/2}$	$1p_{3/2}$	$1p_{1/2}$	$1d_{5/2}$	$1d_{3/2}$	$2s_{1/2}$
$\varepsilon_{\rm GF}$	−20.6035	−13.3109	−13.1363	−6.0358	−5.7893	−5.0977
$\varepsilon_{\rm box}$	−20.6035	−13.3109	−13.1363	−6.0358	−5.7893	−5.0977
(b)	$2p_{3/2}$	$2p_{1/2}$	$1f_{7/2}$	$1f_{5/2}$	$1g_{9/2}$	$1g_{7/2}$
$\varepsilon_{\rm res.}$	0.0774	0.1050	0.6147	0.8215	6.8017	6.9772
Γ	0.1015	0.1259	0.0124	0.0229	3.2003	3.2926

resonant states sit atop of those for free particles. Accordingly, the Λ hyperon bound states are observed in $s_{1/2}$, $p_{1/2}$, $p_{3/2}$, $d_{3/2}$, and $d_{5/2}$ blocks and the resonant states are observed in $p_{1/2}$, $p_{3/2}$, $f_{5/2}$, $f_{7/2}$, $g_{7/2}$, and $g_{9/2}$ blocks.

From the density of states, we can extract the energies for the Λ hyperon bound states and the energies ($\varepsilon_{\rm res.}$) and widths (Γ) for the resonant states. Here, $\varepsilon_{\rm res.}$ and Γ are defined as the positions and the FWHM of resonant peaks, which are the differences between the density of states for the Λ hyperon in ${}^{61}_{\Lambda}$Ca and free hyperon. We list in part (a) of Table I the s.p. energies ε for bound states, in comparison with those obtained by the shooting method with box boundary condition, and in part (b) the energies $\varepsilon_{\rm res.}$ and widths Γ of resonant states. From Table I, it can be seen that s.p. energies for bound states obtained by the Green's function method and shooting method are equal. Six resonant states with very different widths are obtained. Very close to the continuum threshold, resonant states $2p_{1/2}$ and $2p_{3/2}$ with width $\Gamma \sim 0.1$ MeV are observed, and at slightly higher energy around 0.6–0.8 MeV, very narrow resonant states $1f_{5/2}$ and $1f_{7/2}$ with $\Gamma \sim 0.02$ MeV are observed. The behaviors of these narrow resonant states are similar to those of bound states. At very high energy regions, much wider resonant states $1g_{9/2}$ and $1g_{7/2}$ with $\Gamma > 1.1$ MeV are observed; their properties are similar to those of nonresonant scattering states.

To see the distributions of the Λ hyperon resonant states given in Table I, we show in Fig. 4 the integrands for the density of states $n_\kappa(\varepsilon)$, i.e., $\mathrm{Im}[\mathcal{G}_\kappa^{(11)}(r,r;\varepsilon+i\epsilon)+\mathcal{G}_\kappa^{(22)}(r,r;\varepsilon+i\epsilon)]$, in Eq. (17) at the resonant energies. The integrand $\mathrm{Im}[\mathcal{G}_\kappa^{(11)}(r,r;\varepsilon+i\epsilon)+\mathcal{G}_\kappa^{(22)}(r,r;\varepsilon+i\epsilon)]$, which is calculated from the s.p. wave functions with Eq. (18), corresponds to the particle density $\rho_{V\Lambda}$ of Eq. (14b) at energy ε. From Fig. 4, it can be seen that the integrands of the resonant states with the same angular momentum l have very similar distributions and very different for those with different l. The distributions of the resonant states are tightly related to their widths. For the $2p$ resonant states, the distributions at resonant energies are very extended and have large components at coordinate space with $r > 5$ fm. On the contrary, for the very narrow $1f_{5/2}$ and $1f_{7/2}$ resonant states, the density at resonant energy is mainly localized around the surface, i.e., $2.5 < r < 7.5$ fm with a maximum around $r = 5$ fm, the behaviors are very similar to bound state; and for the very wide $1g_{7/2}$ and $1g_{9/2}$ resonant states, the distribution is scattering and outgoing, the behaviors

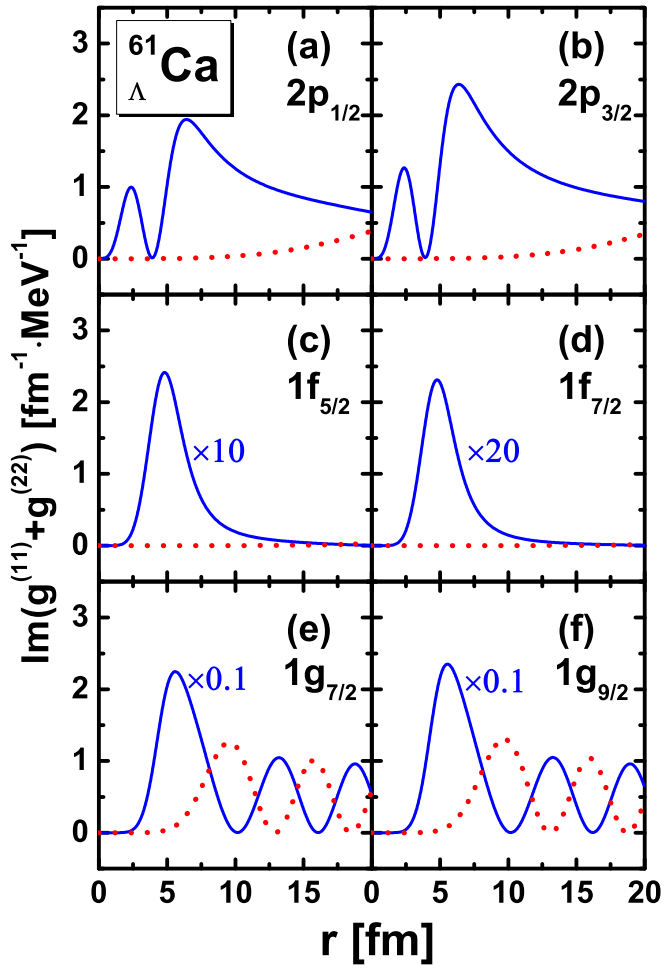

FIG. 4. Integrands for the density of states, $\mathrm{Im}[\mathcal{G}_\kappa^{(11)}(r,r;\varepsilon+i\epsilon)+\mathcal{G}_\kappa^{(22)}(r,r;\varepsilon+i\epsilon)]$, in Eq. (17) at resonant energy $\varepsilon = \varepsilon_{\rm res.}$ for the single-Λ resonant states (a) $2p_{1/2}$, (b) $2p_{3/2}$, (c) $1f_{5/2}$, (d) $1f_{7/2}$, (e) $1g_{7/2}$, and (f) $1g_{9/2}$ in ${}^{61}_{\Lambda}$Ca (blue solid line), in comparison with those for the free particles obtained with $V = S = 0$ (red dotted line). The values of $\varepsilon_{\rm res.}$ are listed in Table I. The integrands for $1f_{5/2}$, $1f_{7/2}$, $1g_{7/2}$, and $1g_{9/2}$ are divided by a factor of 10, 20, 0.1, and 0.1, respectively.

are very similar to the nonresonant scattering states shown by the red dotted lines.

It is well known that neutrons, protons, and Λ hyperons obey their own Pauli principle since they are different fermions. However, in the self-consistent RMF model, Λ hyperon is glue-like and will influence the properties of nucleons. In this section, taking ^{60}Ca, ${}^{61}_{\Lambda}$Ca, and ${}^{62}_{2\Lambda}$Ca as examples, we investigate the influences of Λ hyperons on the single-neutron resonant states. In Table II, the energies $\varepsilon_{\rm res.}$ and widths Γ of the single-neutron resonant states in these (hyper)nuclei obtained by the RMF-GF method are listed. Four single-neutron resonant states $1g_{9/2}$, $2d_{5/2}$, $1g_{7/2}$, and $1h_{11/2}$ are obtained, and their energies $\varepsilon_{\rm res.}$ and widths Γ decrease with the increase of the number of Λ hyperons except for state $1g_{7/2}$ in which these properties increases slightly.

To investigate the changes of the single-neutron resonant states brought by adding Λ hyperons to ^{60}Ca shown in

TABLE II. Comparison of the energies $\varepsilon_{\text{res.}}$ and widths Γ of the single-neutron resonant states in (hyper)nuclei ^{60}Ca, $^{61}_{\Lambda}$Ca, and $^{62}_{2\Lambda}$Ca obtained by RMF-GF method. All quantities are in MeV.

		$1g_{9/2}$	$2d_{5/2}$	$1g_{7/2}$	$1h_{11/2}$
^{60}Ca	$\varepsilon_{\text{res.}}$	0.7656	1.0722	5.4906	10.4430
	Γ	0.0012	0.4134	0.8710	1.9785
$^{61}_{\Lambda}$Ca	$\varepsilon_{\text{res.}}$	0.6679	1.0497	5.4978	10.3981
	Γ	0.0009	0.3915	0.8746	1.9710
$^{62}_{2\Lambda}$Ca	$\varepsilon_{\text{res.}}$	0.5703	1.0260	5.5049	10.3526
	Γ	0.0007	0.3712	0.8795	1.9644

Table II, the mean field potential $V + S$ as well as the s.p. levels including the bound states and resonant states for neutrons in (hyper)nuclei ^{60}Ca, $^{61}_{\Lambda}$Ca, and $^{62}_{2\Lambda}$Ca are plotted in Fig. 5. Adding more Λ hyperons depresses the central part of the neutron mean field potential by around 1.5 MeV per hyperon due to the attractive ΛN interaction. As a result, the s.p. levels for neutrons go down with the increase of the number of Λ hyperons.

Finally, the energy level structures for Λ hyperons are studied. In Fig. 6, we plot the single-Λ energies ε_{Λ} for the Ca hypernucleus isotopes as a function of the mass number A. It can be seen that with increasing hypernuclei mass, the s.p. levels for Λ hyperon go down. Obvious shell gaps are found for Λ hyperon s.p. levels. Besides, the spin-orbit splitting between the spin doublet states $1p$, $1d$, $1f$, and $1g$ are much smaller than those for nucleons shown in Fig. 5. Experimentally, the

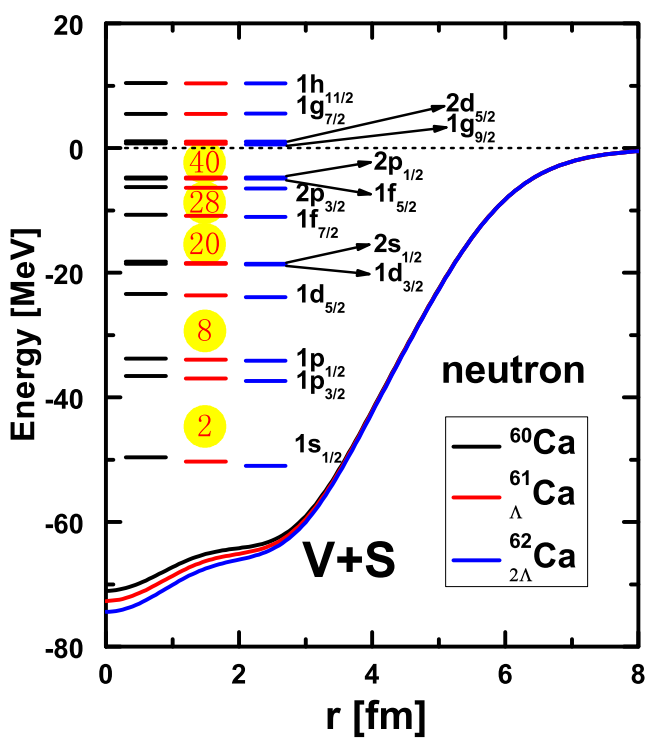

FIG. 5. Mean field potentials $V(r) + S(r)$ as well as the s.p. levels for neutrons in (hyper)nuclei ^{60}Ca, $^{61}_{\Lambda}$Ca, and $^{62}_{2\Lambda}$Ca obtained by RMF-GF method.

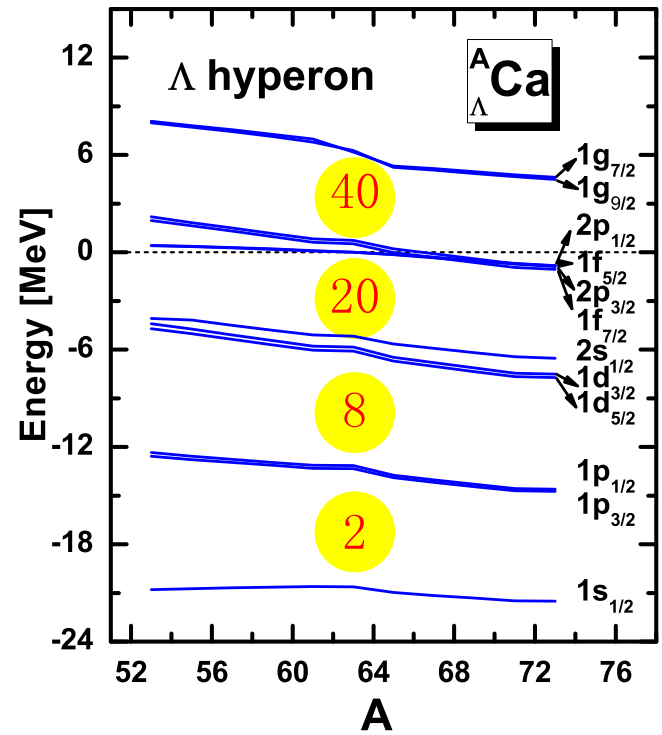

FIG. 6. Evolution of the s.p. levels for the Λ hyperon in the Ca isotopes as a function of mass number A calculated by RMF-GF method.

spin-orbit splitting between the $1p_{1/2}$ and the $1p_{3/2}$ hyperon states in $^{13}_{\Lambda}$C was found to be much smaller than the spin-orbit splitting in ordinary nuclei by a factor of 20–30 [108]. Other experiments [52] reached the same conclusion. Our present results are consistent with those experimental data. In Fig. 6, low-lying $2p$ orbits are found in the continuum, which play important roles in forming hyperon halos. In Ref. [24], the hyperon halo in $^{15}_{3\Lambda}$C and $^{16}_{4\Lambda}$C is predicted by the relativistic continuum Hartree-Bogoliubov theory and caused by the occupation of the weakly bound state $1p_{3/2}$ with extended density distributions and small separation energy of the Λ hyperons. According to those studies, we prefer to say that the hyperon halo may appear in the Ca hypernucleus isotopes due to the low-lying or weakly bound $2p$ orbits.

V. SUMMARY

In this work, the RMF theory with Green's function method in coordinate space is extended to investigate Λ hypernuclei. Detailed formulas are presented.

First, taking $^{61}_{\Lambda}$Ca as an example, the RMF-GF model is applied to study the single-Λ resonant states. By analyzing the density of states, the s.p. energies for bound states and energies and widths for the resonant states are obtained. Consistent results for the single-Λ bound states between the Green's function method and shooting method are obtained. Six resonant states are observed with very different widths, and the distributions of the very narrow $1f_{5/2}$ and $1f_{7/2}$ states are very similar to bound states while the distributions of the wide $1g_{7/2}$ and $1g_{9/2}$ states are like scattering states.

Second, taking ^{60}Ca, $^{61}_{\Lambda}$Ca, and $^{62}_{2\Lambda}$Ca as examples, we investigate the influence of Λ hyperons on single-neutron resonant states and found that for most resonant states, with the increase of the number of Λ hyperons, both the energies and widths decrease due to the deeper mean field potential.

Finally, the s.p. level for Λ hyperon in the Ca isotopes are studied. Obvious shell structure is found for Λ hyperon and very small spin-orbit splitting is obtained, which is consistent with the present experimental results.

ACKNOWLEDGMENTS

This work was partly supported by the National Natural Science Foundation of China (Grants No. 11175002, No. 11335002, No. 11505157, No. 11675148, and No. 11105042).

[1] M. Danysz and J. Pniewski, Philos. Mag. **44**, 348 (1953).
[2] H. Hotchi, T. Nagae, H. Outa, H. Noumi, M. Sekimoto, T. Fukuda, H. Bhang, Y. D. Kim, J. H. Kim, H. Park *et al.*, Phys. Rev. C **64**, 044302 (2001).
[3] O. Hashimoto and H. Tamura, Prog. Part. Nucl. Phys. **57**, 564 (2006).
[4] T. Nagae, Prog. Theor. Phys. Suppl. **185**, 299 (2010).
[5] F. Garibaldi, O. Hashimoto, J. J. LeRose, P. Markowitz, S. N. Nakamura, J. Reinhold, and L. Tang, J. Phys: Conf. Ser. **299**, 012013 (2011).
[6] J. Hao, T. T. S. Kuo, A. Reuber, K. Holinde, J. Speth, and D. J. Millener, Phys. Rev. Lett. **71**, 1498 (1993).
[7] Z.-Y. Ma, J. Speth, S. Krewald, B.-Q. Chen, and A. Reuber, Nucl. Phys. A **608**, 305 (1996).
[8] Y. Tzeng, S. Y. T. Tzeng, and T. T. S. Kuo, Phys. Rev. C **65**, 047303 (2002).
[9] E. Hiyama, T. Motoba, T. A. Rijken, and Y. Yamamoto, Prog. Theor. Phys. Suppl. **185**, 1 (2010).
[10] F. Hofmann, C. M. Keil, and H. Lenske, Phys. Rev. C **64**, 025804 (2001).
[11] J. Schaffner-Bielich, Nucl. Phys. A **804**, 309 (2008).
[12] J. Schaffner-Bielich, Nucl. Phys. A **835**, 279 (2010).
[13] I. Vidaña, Nucl. Phys. A **914**, 367 (2013).
[14] H. Takahashi, J. K. Ahn, H. Akikawa, S. Aoki, K. Arai, S. Y. Bahk, K. M. Baik, B. Bassalleck, J. H. Chung, M. S. Chung *et al.*, Phys. Rev. Lett. **87**, 212502 (2001).
[15] T. Motoba, H. Bandō, and K. Ikeda, Prog. Theor. Phys. **70**, 189 (1983).
[16] E. Hiyama, M. Kamimura, K. Miyazaki, and T. Motoba, Phys. Rev. C **59**, 2351 (1999).
[17] E. Hiyama, M. Kamimura, Y. Yamamoto, and T. Motoba, Phys. Rev. Lett. **104**, 212502 (2010).
[18] B.-N. Lu, E.-G. Zhao, and S.-G. Zhou, Phys. Rev. C **84**, 014328 (2011).
[19] B.-N. Lu, E. Hiyama, H. Sagawa, and S.-G. Zhou, Phys. Rev. C **89**, 044307 (2014).
[20] E. Hiyama, M. Kamimura, T. Motoba, T. Yamada, and Y. Yamamoto, Phys. Rev. C **53**, 2075 (1996).
[21] D. Vretenar, W. Pöschl, G. A. Lalazissis, and P. Ring, Phys. Rev. C **57**, R1060 (1998).
[22] H.-F. Lü, J. Meng, S. Q. Zhang, and S.-G. Zhou, Eur. Phys. J. A **17**, 19 (2003).
[23] X.-R. Zhou, A. Polls, H.-J. Schulze, and I. Vidaña, Phys. Rev. C **78**, 054306 (2008).
[24] H.-F. Lü and J. Meng, Chin. Phys. Lett. **19**, 1775 (2002).
[25] T. Motoba, H. Bandō, K. Ikeda, and T. Yamada, Prog. Theor. Phys. Suppl. **81**, 42 (1985).
[26] H. Bandō, T. Motoba, and J. Žofka, Int. J. Mod. Phys. A **05**, 4021 (1990).
[27] M. Isaka, M. Kimura, A. Dote, and A. Ohnishi, Phys. Rev. C **83**, 044323 (2011).
[28] M. Isaka, H. Homma, M. Kimura, A. Doté, and A. Ohnishi, Phys. Rev. C **85**, 034303 (2012).
[29] M. Isaka, M. Kimura, A. Doté, and A. Ohnishi, Phys. Rev. C **87**, 021304 (2013).
[30] M. Isaka, K. Fukukawa, M. Kimura, E. Hiyama, H. Sagawa, and Y. Yamamoto, Phys. Rev. C **89**, 024310 (2014).
[31] A. Gal, J. M. Soper, and R. H. Dalitz, Ann. Phys. (N.Y.) **63**, 53 (1971).
[32] R. H. Dalitz and A. Gal, Ann. Phys. (N.Y.) **116**, 167 (1978).
[33] D. J. Millener, Nucl. Phys. A **804**, 84 (2008).
[34] D. J. Millener, Nucl. Phys. A **914**, 109 (2013).
[35] M. Rayet, Ann. Phys. (N.Y.) **102**, 226 (1976).
[36] M. Rayet, Nucl. Phys. A **367**, 381 (1981).
[37] Y. Yamamoto, H. Bandō, and J. Žofka, Pro. Theor. Phys. **80**, 757 (1988).
[38] X.-R. Zhou, H.-J. Schulze, H. Sagawa, C.-X. Wu, and E.-G. Zhao, Phys. Rev. C **76**, 034312 (2007).
[39] M. T. Win, K. Hagino, and T. Koike, Phys. Rev. C **83**, 014301 (2011).
[40] R. Brockmann and W. Weise, Phys. Lett. B **69**, 167 (1977).
[41] A. Bouyssy, Phys. Lett. B **99**, 305 (1981).
[42] J. Mareš and B. K. Jennings, Phys. Rev. C **49**, 2472 (1994).
[43] Y. Sugahara and H. Toki, Prog. Theor. Phys. **92**, 803 (1994).
[44] M. T. Win and K. Hagino, Phys. Rev. C **78**, 054311 (2008).
[45] R. Wirth, D. Gazda, P. Navratil, A. Calci, J. Langhammer, and R. Roth, Phys. Rev. Lett **113**, 192502 (2014).
[46] B. D. Serot and J. D. Walecka, Adv. Nucl. Phys. **16**, 1 (1986).
[47] P.-G. Reinhard, Rep. Prog. Phys. **52**, 439 (1989).
[48] P. Ring, Prog. Part. Nucl. Phys. **37**, 193 (1996).
[49] D. Vretenar, A. V. Afanasjev, G. A. Lalazissis, and P. Ring, Phys. Rep. **409**, 101 (2005).
[50] J. Meng, H. Toki, S.-G. Zhou, S. Q. Zhang, W. H. Long, and L. S. Geng, Prog. Part. Nucl. Phys. **57**, 470 (2006).
[51] J. Meng and S.-G. Zhou, J. Phys. G: Nucl. Part. Phys. **42**, 093101 (2015).
[52] W. Brückner, M. A. Faessler, T. J. Ketel, K. Kilian, J. Niewisch, B. Pietrzyk, B. Povh, H. G. Ritter, M. Uhrmacher, P. Birien *et al.*, Phys. Lett. B **79**, 157 (1978).
[53] J. Boguta and S. Bohrmann, Phys. Lett. B **102**, 93 (1981).
[54] R. Brockmann and W. Weise, Nucl. Phys. A **355**, 365 (1981).
[55] M. Rufa, H. Stöcker, J. Maruhn, P.-G. Reinhard, and W. Greiner, J. Phys. G **13**, L143 (1987).
[56] J. Mareš and J. Žofka, Z. Phys. A **333**, 209 (1989).
[57] J. Mareš and J. Žofka, Phys. Lett. B **249**, 181 (1990).
[58] M. Rufa, J. Schaffner, J. Maruhn, H. Stöcker, W. Greiner, and P.-G. Reinhard, Phys. Rev. C **42**, 2469 (1990).
[59] M. Chiapparini, A. O. Gattone, and B. K. Jennings, Nucl. Phys. A **529**, 589 (1991).

[60] J. Schaffner, C. Greiner, and H. Stöcker, Phys. Rev. C **46**, 322 (1992).
[61] J. Schaffner, C. B. Dover, A. Gal, C. Greiner, D. J. Millener, and H. Stöcker, Ann. Phys. (N.Y.) **235**, 35 (1994).
[62] T. T. Sun, E. Hiyama, H. Sagawa, H.-J. Schulze, and J. Meng, Phys. Rev. C **94**, 064319 (2016).
[63] J. Dobaczewski, W. Nazarewicz, T. R. Werner, J. F. Berger, C. R. Chinn, and J. Dechargé, Phys. Rev. C **53**, 2809 (1996).
[64] J. Meng and P. Ring, Phys. Rev. Lett. **77**, 3963 (1996).
[65] N. Sandulescu, L. S. Geng, H. Toki, and G. C. Hillhouse, Phys. Rev. C **68**, 054323 (2003).
[66] W. Pöschl, D. Vretenar, G. A. Lalazissis, and P. Ring, Phys. Rev. Lett. **79**, 3841 (1997).
[67] J. Meng and P. Ring, Phys. Rev. Lett. **80**, 460 (1998).
[68] J. Meng, H. Toki, J. Y. Zeng, S. Q. Zhang, and S.-G. Zhou, Phys. Rev. C **65**, 041302 (2002).
[69] S. Q. Zhang, J. Meng, and S.-G. Zhou, Sci. China-Phys. Mech. Astron. **46**, 632 (2003).
[70] J. Terasaki, S. Q. Zhang, S.-G. Zhou, and J. Meng, Phys. Rev. C **74**, 054318 (2006).
[71] M. Grasso, S. Yoshida, N. Sandulescu, and N. Van Giai, Phys. Rev. C **74**, 064317 (2006).
[72] I. Hamamoto, Phys. Rev. C **81**, 021304 (2010).
[73] S.-G. Zhou, J. Meng, P. Ring, and E.-G. Zhao, Phys. Rev. C **82**, 011301 (2010).
[74] E. P. Wigner and L. Eisenbud, Phys. Rev. **72**, 29 (1947).
[75] J. R. Taylor, *Scattering Theory: The Quantum Theory on Nonrelativistic Collisions* (Wiley, New York, 1972).
[76] G. M. Hale, R. E. Brown, and N. Jarmie, Phys. Rev. Lett. **59**, 763 (1987).
[77] J. Humblet, B. W. Filippone, and S. E. Koonin, Phys. Rev. C **44**, 2530 (1991).
[78] L.-G. Cao and Z.-Y. Ma, Phys. Rev. C **66**, 024311 (2002).
[79] Z. P. Li, J. Meng, Y. Zhang, S.-G. Zhou, and L. N. Savushkin, Phys. Rev. C **81**, 034311 (2010).
[80] B.-N. Lu, E.-G. Zhao, and S.-G. Zhou, Phys. Rev. Lett. **109**, 072501 (2012).
[81] B.-N. Lu, E.-G. Zhao, and S.-G. Zhou, Phys. Rev. C **88**, 024323 (2013).
[82] A. U. Hazi and H. S. Taylor, Phys. Rev. A **1**, 1109 (1970).
[83] Y. K. Ho, Phys. Rep. **99**, 1 (1983).
[84] V. I. Kukulin, V. M. Krasnopl'sky, and J. Horácek, *Theory of Resonances: Principles and Applications* (Kluwer Academic, Dordrecht, 1989).
[85] S.-C. Yang, J. Meng, and S.-G. Zhou, Chin. Phys. Lett. **18**, 196 (2001).
[86] S. S. Zhang, J. Meng, S.-G. Zhou, and G. C. Hillhouse, Phys. Rev. C **70**, 034308 (2004).
[87] J.-Y. Guo, R. D. Wang, and X. Z. Fang, Phys. Rev. C **72**, 054319 (2005).
[88] J.-Y. Guo and X. Z. Fang, Phys. Rev. C **74**, 024320 (2006).
[89] L. Zhang, S.-G. Zhou, J. Meng, and E.-G. Zhao, Phys. Rev. C **77**, 014312 (2008).
[90] J.-Y. Guo, X.-Z. Fang, P. Jiao, J. Wang, and B.-M. Yao, Phys. Rev. C **82**, 034318 (2010).
[91] T. T. Sun, S. Q. Zhang, Y. Zhang, J. N. Hu, and J. Meng, Phys. Rev. C **90**, 054321 (2014).
[92] T. T. Sun, Z. M. Niu, and S. Q. Zhang, J. Phys. G: Nucl. Part. Phys. **43**, 045107 (2016).
[93] S. T. Belyaev, A. V. Smirnov, S. V. Tolokonnikov, and S. A. Fayans, Sov. J. Nucl. Phys. **45**, 783 (1987).
[94] E. N. Economou, *Green's Fucntion in Quantum Physics* (Springer-Verlag, Berlin, 2006).
[95] H. Oba and M. Matsuo, Phys. Rev. C **80**, 024301 (2009).
[96] Y. Zhang, M. Matsuo, and J. Meng, Phys. Rev. C **83**, 054301 (2011).
[97] Y. Zhang, M. Matsuo, and J. Meng, Phys. Rev. C **86**, 054318 (2012).
[98] T. T. Sun, M. Matsuo, Y. Zhang, and J. Meng, arXiv:1310.1661.
[99] M. Matsuo, Nucl. Phys. A **696**, 371 (2001).
[100] M. Matsuo, Prog. Theor. Phys. Suppl. **146**, 110 (2002).
[101] J. Daoutidis and P. Ring, Phys. Rev. C **80**, 024309 (2009).
[102] D. Yang, L.-G. Cao, Y. Tian, and Z.-Y. Ma, Phys. Rev. C **82**, 054305 (2010).
[103] A. C. Mueller, Prog. Part. Nucl. Phys. **46**, 359 (2001).
[104] J. V. Noble, Phys. Lett. B **89**, 325 (1980).
[105] W. H. Long, J. Meng, N. Van Giai, and S.-G. Zhou, Phys. Rev. C **69**, 034319 (2004).
[106] Q. N. Usmani and A. R. Bodmer, Phys. Rev. C **60**, 055215 (1999).
[107] C. B. Dover and A. Gal, Prog. Part. Nucl. Phys. **12**, 171 (1984).
[108] S. Ajimura, H. Hayakawa, T. Kishimoto, H. Kohri, K. Matsuoka, S. Minami, T. Mori, K. Morikubo, E. Saji, A. Sakaguchi *et al.*, Phys. Rev. Lett. **86**, 4255 (2001).